JACS
JOURNAL OF THE AMERICAN CHEMICAL SOCIETY
Article
pubs.acs.org/JACS

Tuning the Reactivity of Terminal Nickel(III)−Oxygen Adducts for C−H Bond Activation

Paolo Pirovano,[†] Erik R. Farquhar,[‡] Marcel Swart,[§,∥] and Aidan R. McDonald*[,†]

[†]School of Chemistry and CRANN/AMBER Nanoscience Institute, Trinity College Dublin, The University of Dublin, College Green, Dublin 2, Ireland

[‡]Case Western Reserve University Center for Synchrotron Biosciences, National Synchrotron Light Source II, Brookhaven National Laboratory, Upton, New York 11973, United States

[§]ICREA, Pg. Lluís Companys 23, 08010 Barcelona, Spain

[∥]Institut de Química Computacional i Catàlisi, Facultat de Ciències, Universitat de Girona, Campus Montilivi, 17003 Girona, Spain

Supporting Information

ABSTRACT: Two metastable Ni^{III} complexes, $[Ni^{III}(OAc)(L)]$ and $[Ni^{III}(ONO_2)(L)]$ (L = *N*,*N*′-(2,6-dimethylphenyl)-2,6-pyridinedicarboxamidate, OAc = acetate), were prepared, adding to the previously prepared $[Ni^{III}(OCO_2H)(L)]$, with the purpose of probing the properties of terminal late-transition metal oxidants. These high-valent oxidants were prepared by the one-electron oxidation of their Ni^{II} precursors ($[Ni^{II}(OAc)(L)]^-$ and $[Ni^{II}(ONO_2)(L)]^-$) with tris(4-bromophenyl)ammoniumyl hexachloroantimonate. Fascinatingly, the reaction between any $[Ni^{II}(X)(L)]^-$ and NaOCl/acetic acid (AcOH) *or* cerium ammonium nitrate ($(NH_4)_2[Ce^{IV}(NO_3)_6]$, CAN), yielded $[Ni^{III}(OAc)(L)]$ and $[Ni^{III}(ONO_2)(L)]$, respectively. An array of spectroscopic characterizations (electronic absorption, electron paramagnetic resonance, X-ray absorption spectroscopies), electrochemical methods, and computational predictions (density functional theory) have been used to determine the structural, electronic, and magnetic properties of these highly reactive metastable oxidants. The Ni^{III}-oxidants proved competent in the oxidation of phenols (weak O−H bonds) and a series of hydrocarbon substrates (some with strong C−H bonds). Kinetic investigation of the reactions with di-*tert*-butylphenols showed a 15-fold enhanced reaction rate for $[Ni^{III}(ONO_2)(L)]$ compared to $[Ni^{III}(OCO_2H)(L)]$ and $[Ni^{III}(OAc)(L)]$, demonstrating the effect of electron-deficiency of the O-ligand on oxidizing power. The oxidation of a series of hydrocarbons by $[Ni^{III}(OAc)(L)]$ was further examined. A linear correlation between the rate constant and the bond dissociation energy of the C−H bonds in the substrates was indicative of a hydrogen atom transfer mechanism. The reaction rate with dihydroanthracene (k_2 = 8.1 M^{-1} s^{-1}) compared favorably with the most reactive high-valent metal-oxidants, and showcases the exceptional reactivity of late transition metal−oxygen adducts.

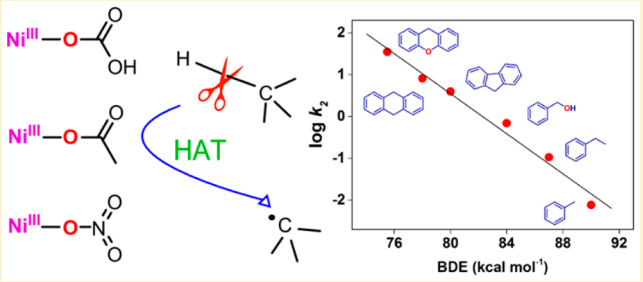

INTRODUCTION

The oxidative functionalization of C−H bonds in inert hydrocarbons represents a powerful transformation. Great economic and environmental value would derive from the possibility of converting readily available feedstock chemicals (i.e., natural gas and petroleum) into higher value oxidized products, while avoiding the currently employed endothermic and energy-intensive processes, such as cracking and dehydrogenation.[1] To this end, catalysts based on cheap and abundant first-row transition metals are particularly attractive.

Numerous Fe- and Cu-containing metalloenzymes (oxygenases) perform such hydrocarbon oxidations under ambient conditions, selectively producing hydroxylated, halogenated, or desaturated hydrocarbons.[2] It has been determined that in many of these natural and non-natural catalyst systems, activation of the C−H bond in the substrate occurs through hydrogen atom transfer (HAT) brought about by a metal in a high oxidation state with a terminal oxygen ligand.[3] Examples of enzymatic and synthetic high-valent terminal Mn- and Fe-oxo species are abundant,[4] however there remain very few examples of terminal late transition metal−oxygen adducts.

While no examples of terminal Ni- and Cu-oxo complexes have yet been reported, progress has been made in preparing late transition metal oxygen adducts. Tolman and co-workers have explored a unique Cu^{III}−OH complex, which could oxidatively activate strong C−H bonds, at rates that rivalled or surpassed Fe-, Mn-, and Ru-oxo complexes (Table 2).[5] For nickel, in contrast, the scarcity of well-characterized terminal high-valent Ni−O oxidants has posed a problem. We recently reported a Ni^{III}−OCO_2H complex (**1b**, Scheme 1), prepared from **1a**,[6] which we deemed capable of HAT; unfortunately, in

Received: August 11, 2016
Published: October 14, 2016

DOI: 10.1021/jacs.6b08406
J. Am. Chem. Soc. 2016, 138, 14362−14370

Scheme 1. Synthesis of Ni^{II} Complexes 2a, 3a, and 4[a]

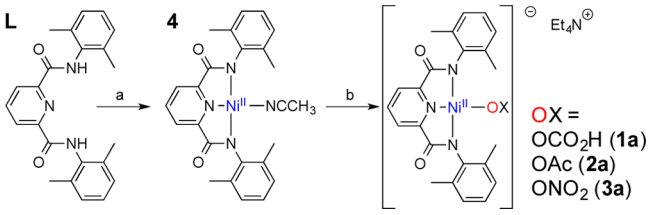

[a](a) (1) $NiCl_2$, CH_3OH, 65 °C; (2) $NaOCH_3$; (3) CH_3CN (b) for **2a**: Et_4NOAc, CH_3CN, Et_2O, room temperature; for **3a**: Et_4NNO_3, CH_3OH, Et_2O, room temperature. The synthesis of **1a** was previously reported.[6a]

the conditions of the study, the reactions were limited to substrates containing weak O−H and C−H bonds.[7] Dinuclear, bridged Ni^{III}_2−μ-$(O)_2$ complexes have also been widely studied, and examples of intramolecular HAT have been observed.[8] Ray observed the formation of multiple metastable putative Ni^{III}−OX species, from the reaction of a Ni^{II} complex and 3-chloroperoxybenzoic acid (*m*-CPBA), and the resulting mixture was capable of oxidizing hydrocarbons with weak C−H bonds (1,4-cyclohexadiene).[9] To date, the most powerful high-valent nickel oxidant, reported by Company, was a putative formally Ni^{IV} species, obtained from the reaction of a macrocyclic Ni^{II} complex with *m*-CPBA.[10] Overall, the Ray/Company species lacked sufficient stability to allow exhaustive characterization. Other terminal Ni^{III}−OX complexes displayed no particular oxidizing power toward C−H bonds.[11]

Experimental and theoretical studies on metal-based oxidants have highlighted several factors that affect the HAT reactivity of these species.[5,12] An important development in the field is the observation that the rate of the reaction is correlated with its thermodynamic driving force.[12c] The existence of a linear relationship between the reaction energy and the activation energy, within a family of simple reactions, was recognized from early kinetic and theoretical studies (Bell−Evans−Polanyi principle).[13] Mayer has applied a Marcus theory based approach to describe the HAT reactivity for metal complexes, from which he rederived the aforementioned relation.[12c,14] In a HAT reaction between a metal−oxygen adduct and a C−H bond, the $\Delta G°$ is equal to the difference between the bond dissociation free energy (BDFE) of the C−H bond that is broken in the substrate and that of the O−H bond that is formed. An important consequence of the linear free energy relationship is that a higher-energy intermediate will display higher reaction rates, as well as provide the driving force for the activation of stronger C−H bonds. High-valent compounds of the later transition metals are destabilized by their higher electronegativity, lower stability of the high oxidation states, and destabilizing interactions between occupied *d*-orbitals and π-donating O ligands; hence, we expect late transition metal oxidants could be powerful reagents.[12a,15]

To this end, we have explored a series of well-defined, well-characterized, highly reactive high-valent nickel−oxygen complexes. Herein, we report the preparation of two new Ni^{III}−OX complexes, $[Ni^{III}(OAc)(L)]$ (**2b**) and $[Ni^{III}(ONO_2)(L)]$ (**3b**), from their Ni^{II}−OX precursors **2a** and **3a**, respectively (Scheme 1, L = *N*,*N*′-(2,6-dimethylphenyl)-2,6-pyridinedicarboxamidate[16]). We present an investigation into relationships between the properties of the O-donor ligands in **1**−**3b** and their oxidative reactivity. Moreover, we demonstrate that $[Ni^{III}(OAc)(L)]$ (**2b**) can oxidize a wide range of hydrocarbon substrates, and is capable of activating very strong C−H bonds, making it one of the most potent high-valent metal-based oxidants reported to date.

RESULTS AND DISCUSSION

Synthesis of $[Ni^{II}(X)(L)]$ Complexes. $Et_4N[Ni^{II}(OAc)(L)]$ (**2a**) and $Et_4N[Ni^{II}(ONO_2)(L)]$ (**3a**) were obtained via a two-step synthesis (Scheme 1). The neutral complex $[Ni^{II}(NCCH_3)(L)]$ (**4**) was first synthesized by reacting LH_2 with $NiCl_2$ (1 equiv) in the presence of $NaOCH_3$ (2.1 equiv), in CH_3OH. Subsequent CH_3CN ligand introduction and filtration of insoluble byproducts allowed for isolation of pure **4**. The product was obtained in 75% yield. The CH_3CN ligand in **4** could be displaced by the addition of either tetraethylammonium acetate (Et_4NOAc, 1.1 equiv) to a CH_3CN solution of **4**, or tetraethylammonium nitrate (Et_4NNO_3, 1.1 equiv) to a CH_3OH solution of **4**, to yield **2a** and **3a**, respectively. ^1H and ^{13}C NMR, attenuated total reflectance Fourier transform infrared (ATR-FTIR), and high resolution electrospray ionization mass spectrometry (ESI-MS) confirmed the structure, composition, and elemental assignments of the complexes.

Single crystals of **2a**, **3a**, and **4** that were suitable for X-ray diffraction (XRD) measurements were obtained (Figure 1). All

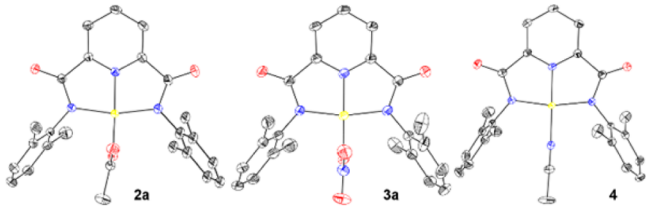

Figure 1. ORTEP plots (at 50% probability level) of the X-ray crystallographically determined structures of **2a**, **3a**, and **4**; hydrogen atoms for all and counterions for **2a** and **3a** have been omitted for clarity.

the complexes showed the Ni^{II} ion to be in a square planar coordination environment. The geometric parameters of the $[Ni^{II}(L)]$ unit were similar to those of previously reported $[Ni^{II}(L)]$ complexes (Table S1).[6a] The ^-OAc and $^-ONO_2$ anions, in **2a** and **3a**, respectively, bind in a monodentate fashion (Figure 1), similarly to the bicarbonate ligand in **1a**,[6a] and lie perpendicular to the [Ni(L)] plane. The XRD experiments confirmed the structure of compounds **2a**, **3a**, and **4**, showing a nearly invariant square planar nickel coordination environment, with bond distances that are largely unaffected by the electron-donating ability of the ancillary ligands.

Preparation and Characterization of $[Ni^{III}(OX)(L)]$ Complexes. We previously reported the generation of $[Ni^{III}(OCO_2H)(L)]$, **1b**, by the one electron oxidation of **1a**.[7] In an analogous fashion, complexes **2a** and **3a** were oxidized to yield $[Ni^{III}(OAc)(L)]$ and $[Ni^{III}(ONO_2)(L)]$, **2b** and **3b**, respectively (Scheme 2). This was achieved by dissolving **2a** and **3a** in acetone (0.3 mM) and cooling these solutions to −40 °C. Addition of 1 equiv of the one-electron oxidant tris(4-bromophenyl)ammoniumyl hexachloroantimonate (magic blue, dissolved in CH_3CN) caused an immediate reaction as evidenced by electronic absorption spectroscopy (Figure 2). For both **2a** and **3a**, the immediate appearance of two intense visible and NIR absorption bands in the electronic

DOI: 10.1021/jacs.6b08406
J. Am. Chem. Soc. 2016, 138, 14362−14370

Scheme 2. Synthetic Routes to the Ni^{III} Complexes 1−3b[a]

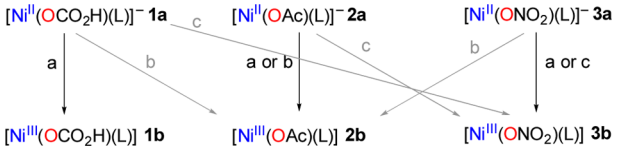

[a](a) Magic blue (1 equiv, acetone); (b) NaOCl/AcOH/H_2O (15 equiv, acetone); (c) $(NH_4)_2Ce(NO_3)_6$ (CAN, 5 equiv, acetone). Gray crossover reactions show that NaOCl/AcOH always yields **2b**, and CAN always yields **3b**.

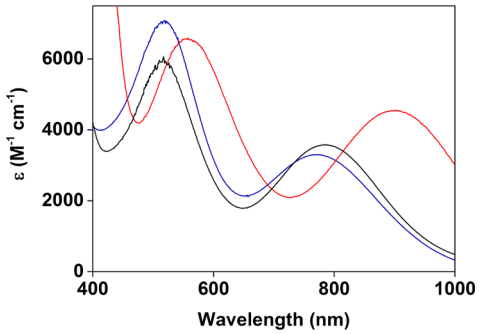

Figure 2. UV−visible spectra of $[Ni^{III}(OX)(L)]$ complexes **1b** (black trace), **2b** (blue trace), and **3b** (red trace), in acetone solutions. Molar absorptivities were calculated using the Beer−Lambert equation from the measured absorbances and EPR-determined concentrations of the products.

absorption spectra, assigned to **2b** and **3b** respectively, demonstrated their one-electron oxidation.

Such features in the visible region have been identified as typical of Ni^{III} complexes of 2,6-pyridinedicarboxamidate ligands.[7,16c] Specifically, **2b** displayed features at λ_{max} = 510 and 760 nm, while **3b** displayed absorption maxima at λ_{max} = 560 and 890 nm (Figure 2). The presence of these features compares favorably to the electronic absorption spectrum of **1b** (λ_{max} = 520 and 780 nm, Figure 2), with only minor differences between the $^{-}OCO_2H$-ligated **1b** and ^{-}OAc-ligated **2b**. In the case of the more electron-poor $^{-}ONO_2$-ligated **3b**, red-shifted absorption features (compared to **1b** and **2b**) were observed, presumably as a result of the $^{-}ONO_2$ ligand being markedly less basic.

We observed that cerium ammonium nitrate ($(NH_4)_2[Ce^{IV}(NO_3)_6]$, CAN) affected the oxidation of **3a** (0.3 mM acetone solution, − 40 °C, 5 equiv of CAN in CH_3OH) to give **3b** as evidenced by electronic absorption spectroscopy and EPR (Figures S19 and 20). Fascinatingly, addition of excess CAN (5 equiv) to either **1a** or **2a**, *also* caused the appearance of the characteristic absorption bands of **3b** (λ_{max} = 560 and 890 nm, Figures S21−22, see the Supporting Information for experimental details), presumably as a result of the large excess of $^{-}ONO_2$ anions in CAN. In a similar way, we could generate species **2b** by oxidizing **2a** with hypochlorous acid (formed from an aqueous NaOCl/AcOH mixture, see the Supporting Information for experimental details), as evidenced by electronic absorption and EPR spectroscopies (Figure S23−24). Furthermore, addition of NaOCl/AcOH to **1a** or **3a** resulted in the formation of features similar to those of **2b** (Figure S25 and 26). In summary, oxidation of the Ni^{II} precursors **1−3a** by magic blue is a method of general validity, while CAN and NaOCl/AcOH could only cleanly generate $^{-}ONO_2$-ligated **3b** and ^{-}OAc-ligated **2b**, respectively. We were surprised to observe the formation of anion-ligated complexes for CAN and NaOCl/AcOH, and find this observation quite intriguing given the wide employment of these oxidants to generate terminal metal-oxo species.

1−3b were thermally unstable: at −40 °C, half-lives ($t_{1/2}$) of 90 min for **1b**[7] and 200 min for **3b** were measured; in contrast, **2b** showed no appreciable decay over the course of several hours at −40 °C. When **2b** was prepared using NaOCl/AcOH it displayed a half-life of 750 s at 25 °C. Neither **1b** nor **3b** were stable at 25 °C.

Electron paramagnetic resonance (EPR) spectroscopy analysis of **2−3b** showed the presence of a single S = 1/2 species for each complex (Figure 3). The spectra displayed axial

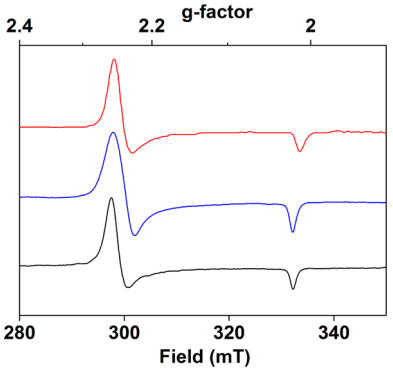

Figure 3. EPR spectra of **1b** (black trace),[7] **2b** (blue trace), and **3b** (red trace), collected from frozen acetone solutions at 77 K, microwave power = 31.6 mW. Simulated spectra can be found in the Supporting Information (Figures S15−17).

symmetry with $g\perp > g_{\parallel}$. The average g-values (g_{av}, Table 1) were consistent with the unpaired electron residing predominantly on the Ni^{III} ion. For **1−3b**, the g-values (Table 1, Figures S15−17) are essentially equivalent, and together with the shape of the signal ($g\perp > g_{\parallel}$) are consistent with a low-spin, d^7 Ni^{III} ion in square planar or elongated octahedral coordination environment.[17] The similarities in g-value are consistent with the XAS-determined metal−ligand bond distances being almost equal for **1−3b**, and suggests little to no difference in electronic symmetry at the metal site.

Density functional theory (DFT) Mulliken spin density calculations were performed and suggested that the unpaired spin in **1−3b** predominantly resides in a metal-based molecular orbital (d_{z2}- or d_{xz}-like molecular orbitals, Table S10). Often when $g\perp \gg g_{\parallel}$, it has been indicative of a d_{z2} singly occupied molecular orbital.[17,18] However, we cannot definitively conclude where the unpaired spin density resides, as detailed below. The yields of the S = 1/2 entities were determined to be ∼95% (±15), through comparison with a spin standard ((2,2,6,6-tetramethylpiperidin-1-yl)oxyl (TEMPO), 0.4 mM), based on the concentration of the Ni^{II} starting solutions. This corresponds to a nearly quantitative conversion of the Ni^{II} precursors to Ni^{III}-oxygen adducts.

ESI-MS analysis was conducted by injecting thawed acetone solutions of **2b** and **3b**, immediately after thawing. In the solution of **2b**, a peak at m/z = 495 was identified that corresponds to a mass of $[\mathbf{2b} + Li^+]^+$ (Figure S18). For **3b**, a mass peak at m/z = 510 was detected (Figure S18), which corresponds to $[\mathbf{3b} + H_3O^+]^+$. The isotopic patterns for the observed ions were typical of Ni-containing ions, demonstrating

DOI: 10.1021/jacs.6b08406
J. Am. Chem. Soc. 2016, 138, 14362−14370

Table 1. Salient Spectroscopic Features and Properties of $[Ni^{II}(L)]$ and $[Ni^{III}(OX)(L)]$

	λ_{max} (nm), (ε/$M^{-1}cm^{-1}$)	$\nu_{C=O/C\equiv N/N=O}$ (cm^{-1})	$g\perp$, $g_{\parallel}$ (g_{av})	$E_{1/2}$ vs Fc^{+}/Fc (V)	Ni−O (Å)	Ni K-pre-edge and -edge (eV)	k_2 2,6-DTBP @ −40 °C ($M^{-1}s^{-1}$)[d]
1a	470 (1200)	1618, 1585		0.48	1.87,[a] 1.878,[b] 1.871[c]	8345	
2a	470 (1200)	1620, 1608, 1585		0.35	1.87,[a] 1.864,[b] 1.870[c]	8333.1, 8345	
3a	455 (1200)	1623, 1609, 1587, 1290		0.56	1.88,[a] 1.890,[b] 1.888[c]	8332.7, 8345	
1b	520 (6000), 780 (3600)		2.25, 2.02 (2.17)		1.84,[a] 1.944/2.146,[be] or 1.874,[bf]	8345	0.104
2b	510 (7000), 760 (3300)		2.24, 2.02 (2.17)		1.92,[a] 1.929/2.118,[be] or 1.864[bf]	8333.6, 8345	0.125
3b	560 (6700), 890 (4600)		2.25, 2.01 (2.17)		1.93/2.08,[a] 1.944/2.108,[be] or 1.888[bf]	8333.8, 8345	1.96
4	435 (1400), 550 (110)	2337, 2311, 1630, 1585					

[a]From EXAFS fitting. [b]From DFT. [c]From XRD. [d]Second order rate constant for the reaction with 2,6-di-*tert*-butylphenol at −40 °C. [e]d_{z2} spin-density. [f]d_{xz} spin density.

the ions are likely to be the expected Ni^{III} products (simulated spectra in Figure S18). It should be noted that in the ESI-MS analysis of solutions of the Ni^{II} precursors **2**−**3a**, *only* negatively charged ions could be detected, meaning ESI-MS of the Ni^{II} precursor results in the anionic $[Ni^{II}(OX)(L)]^{-}$ fragment flying. ESI-MS analysis of the Ni^{III} products **2**−**3b** displayed the positively charged ions discussed above. This means that the ESI-MS analysis of **2**−**3b** pertains only to the Ni^{III} oxidation state and not the precursor Ni^{II} species. The low-temperature ESI-MS analysis thus provides proof for the elemental composition of **2** and **3b**.

Neither **2b** nor **3b** were sufficiently thermally stable to grow crystals suitable for X-ray crystallography. Therefore, we performed Ni K-edge X-ray absorption spectroscopy (XAS) on frozen solutions of both complexes. The Ni K-edge energy obtained for both **2b** and **3b** (8345 eV, Table 1) was within the range expected for Ni^{III} ions,[19] and was almost the exact same as that obtained for **1b** (8345 eV).[7] A comparison of the Ni K-edge X-ray absorption near-edge spectra (XANES)(Figures 4 and S44) showed little difference between precursor complexes **1**−**3a**, suggesting that the anionic oxy-donor ligand does not dramatically affect the Ni K-edge energy (Figures 4, S45, and S46, Table 1). As with a comparison of the XANES of **1a** and **1b**,[7] there was little-to-no shift in the Ni K-edge upon comparison of **2**−**3a** with **2**−**3b**, respectively (Table 1, Figure S46). However, the XANES spectra of Ni^{II} complexes **2**−**3a** display a markedly different profile/shape to those of **2**−**3b** (Figure S46), indicating a reaction had occurred upon oxidation of **1**−**3a** to yield **1**−**3b**. Analogous observations that identify no edge energy changes when comparing $Ni^{II/III}$ species, within comparable coordination environments, have previously been observed.[19a,20] In this instance, contributions to the edge from 1*s*-to-4*p* absorption features distort the edge shape (~8340 eV), making determination of nickel oxidation state from edge energy alone challenging. We further note that the weak 1*s*-to-3*d* pre-edge transitions show modest 0.5−1 eV blue shifts (Table 1, Figure S46) upon conversion of **2a** to **2b** (8333.1 to 8333.6 eV) and **3a** to **3b** (8332.7 to 8333.8 eV), providing further evidence for an altered ligand field in **2**−**3b** consistent with an increase in Ni oxidation state.[21]

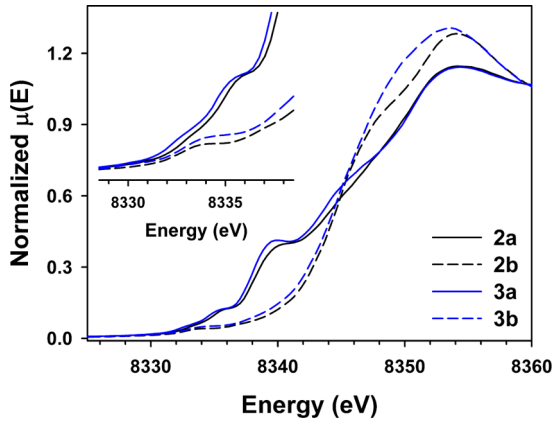

Figure 4. Normalized XANES spectra of complexes **2a**, **2b**, **3a**, and **3b**. The inset shows an expansion of the pre-edge region.

Extended X-ray absorption fine structure (EXAFS) analysis of **2b** and **3b** showed that both contained a first coordination sphere with 4−5 O/N scatterers (Table 1, Tables S5−S8). For **1**−**3b**, there was a small but statistically significant expansion of the average scatterer distance from the absorber (the distance gets longer going from **1b** to **3b**). This would suggest the $^{-}ONO_2$ ligand in **3b** was more weakly bound, and a weaker field donor. For **3b** the best fits were obtained through splitting the first shell, yielding scattering atoms at 1.93 and a rather long 2.08 Å, respectively. The latter shell presumably reflects a $^{-}ONO_2$ ligand bound in a bidentate fashion in **3b**. Fitting the data with a very short Ni−O bond (ca. 1.65 Å) resulted in very poor fits, eliminating the possibility of **1**−**3b** being terminal Ni^{III}=O.

To further understand the structural properties of **2b** and **3b**, we performed DFT calculations using an array of methods (Tables S9−10, Figures S48−S50). First, the DFT-predicted Ni−O bond lengths for **1**−**3a** correlated well with the X-ray crystallographically determined bond lengths, and those measured using XAS. For the Ni^{III} complexes **1**−**3b**, DFT methods suggested negligible difference in relative energy (ca. 1 kcal/mol) for species where the unpaired electron resides in a metal-based d_{xz}- or d_{z2}-like molecular orbital (Table S10). Fascinatingly, dramatic differences in the ligand-binding mode are predicted whether the unpaired electron resides in a d_{xz}- or d_{z2}-like orbital, where the ligands are coordinated either in monodentate (d_{xz}) or bidentate (d_{z2}) fashion (Figures S48−S50). The metal−ligand bond-length predictions are also predicted to be affected by the nature of the binding mode (Table 1). Critically, the XAS-determined Ni−O bond length for **3b** correlates well with that predicted for **3b** with the unpaired electron residing in a d_{z2}-like molecular orbital. The

DOI: 10.1021/jacs.6b08406
J. Am. Chem. Soc. 2016, 138, 14362−14370

XAS thus suggests that in **3b** the $^{-}ONO_2$ ligand may be bidentate, whereas for **1b** and **2b** the ancillary ligands are likely monodentate. DFT predicts negligible energy differences between **1**−**3b** with the respective binding modes, while EPR suggests that for **1**−**3b** the d_{z2} is occupied, and thus all three should have bidentate donors. Overall, the DFT calculations correlate well with the XAS-determined bond lengths, although the binding mode for the ancillary O-donor ligands remains unclear. Importantly, the $^{-}ONO_2$ ligand in **3b** appears to be the weakest-field donor, causing **3b** to be the most electrophilic oxidant.

Reactivity Studies. *Phenol oxidation.* In order to ascertain the effect of varying the oxygen-adduct (i.e., $^{-}OCO_2H$ for **1b**, ^{-}OAc for **2b**, $^{-}ONO_2$ for **3b**), we performed the reaction between 2,6-di-*tert*-butylphenol (2,6-DTBP, in excess) and **2b** and **3b** at −40 °C. We previously demonstrated that **1b** reacted with 2,6-DTBP at −40 °C.[7] In order to ensure a fair/effective comparison, we used magic blue as the oxidant in the preparation of **2b** and **3b** (as was the case for **1b**), and the same reaction temperature (−40 °C) and solvent medium (acetone) was used for all three reactivity studies.

The reactions between **2b** and **3b** and 2,6-DTBP were monitored by electronic absorption spectroscopy: upon addition of an excess of substrate (>10 equiv 2,6-DTBP) to 0.3 mM solutions of **2b** and **3b** in acetone, decay of the absorbance features attributed to **2b** and **3b** was observed. After the reactions, the radical homocoupling product 3,3′,5,5′-tetra-tert-butyl-[1,1′-bis(cyclohexane)]-2,2′,5,5′-tetraene-4,4′-dione, together with small amounts of its hydroquinoid form 3,3′,5,5′-tetra-tert-butyl-[1,1′-biphenyl]-4,4′-diol (Scheme S1), were detected by ESI-MS. The decay was monitored over the course of the reaction, and pseudo first order rate constants (k_{obs}) were obtained by exponential fitting of the decay plot. Second-order rate constants (k_2) were determined by plotting k_{obs} (determined at varying substrate concentrations) against substrate concentration and calculating the slope of the resulting linear plot (Figure 5). The reactions of **2b** and **3b** with 2,6-DTBP proceeded with k_2 of 0.125 and 1.96 M^{-1} s^{-1}, respectively (Table S3). The k_2 determined for **2b** was thus comparable with that measured for **1b** (k_2 = 0.104 M^{-1} s^{-1}), while that determined for **3b** was approximately 15 times greater. The $^{-}ONO_2$ ligand thus appears to enhance the oxidative reactivity of **3b** by an order of magnitude compared to the terminal $^{-}OCO_2H$ and ^{-}OAc ligands in **1b** and **2b**.

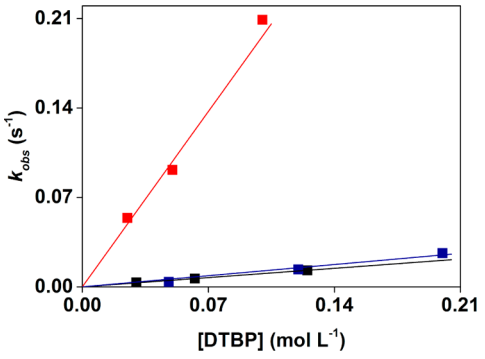

Figure 5. Plots of k_{obs} versus [2,6-DTBP] determined for the reaction between **1b** (black), **2b** (blue), and **3b** (red) and 2,6-DTBP at −40 °C in acetone.

We also determined k_2 for the reaction of **3b** with 2,4-di-*tert*-butylphenol (2,4-DTBP, k_2 = 158 M^{-1} s^{-1}), which was 80 times larger than that of 2,6-DTBP (Figure S28). Importantly, different reaction kinetics between these two sterically disparate substrates by the same oxidant has been considered to imply a HAT mechanism.[12d] Furthermore, a kinetic isotope effect for the reaction of **1b** with 2,6-DTBP of 2.1 was previously measured.[7] These rate constants and KIE values are a strong indication that **1**−**3b** perform HAT, rather than another form of proton coupled electron transfer (PCET) on phenols.

Mayer and co-workers have been to the fore in defining the HAT reactivity properties of metal-based oxidants.[12c,14,22] They have demonstrated that thermodynamic driving forces (ΔG of the HAT reaction) determine the reactivity properties of metal-based oxidants. In the HAT reactions between **1**−**3b** and 2,6-DTBP, ΔG would explicitly be correlated to the BDFE of the newly formed O−H bond in the $[Ni^{II}(O(H)X)(L)]$ products (defined as **1**−**3a(H)**). The $BDFE_{O-H}$ can be defined as the sum of the free energies of two steps (plus a constant), $[Ni^{III}(OX)(L)]$ (**1**−**3b**) + e^- → $[Ni^{II}(OX)(L)]^-$ (**1**−**3a**) and $[Ni^{II}(OX)(L)]^-$ (**1**−**3a**) + H^+ → $[Ni^{II}(O(H)X)(L)]$ (**1**−**3a(H)**), which are represented by $E^0_{Ni(II/III)}$ of **1**−**3a** and the $pK_{a(O-H)}$ of **1**−**3a(H)**, respectively. We have endeavored to calculate the $BDFE_{O-H}$ for **1**−**3a(H)** by obtaining $E^0_{Ni(II/III)}$ for **1**−**3a** and a $pK_{a(O-H)}$ for **1**−**3a(H)**.

Cyclic voltammograms for solutions of **1**−**3a** in acetone (Bu_4NPF_6 (0.1 M, Bu_4N = tetrabutylammonium), scan rate of 0.05 V/s) displayed quasi-reversible ($\Delta E_{pa,pc}$: **1a**, 0.11 V; **2a**, 0.07 V; **3a**, 0.13 V) redox waves at $E_{1/2}$ = 0.48, 0.35, and 0.56 V vs Fc^+/Fc respectively (Figure 6, Fc = ferrocene). The measured $E^0_{Ni(II/III)}$ for **1**−**3a** showed the expected correlation with the electronic properties of the terminal ligands, i.e. the more basic ligands yielded complexes with smaller $E^0_{Ni(II/III)}$ (^{-}OAc < $^{-}OCO_2H$ < $^{-}ONO_2$). A comparison of the pK_a of the conjugate acids of the ligands showed that the $^{-}OCO_2H$ and ^{-}OAc ligands have similar values (aqueous scale pK_a of AcOH = 4.7, H_2CO_3 = 3.5).[23] In contrast the $^{-}ONO_2$ ligand is much more electron-poor (aqueous scale pK_a of HNO_3 = −1.2).[24] The most electrophilic Ni^{III}-oxygen adduct is therefore likely to be **3b**, based on the $E^0_{Ni(II/III)}$ for **3a**.

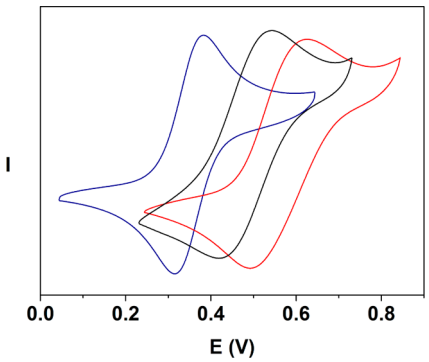

Figure 6. Steady state cyclic voltammograms of **1a** (black), **2a** (blue), and **3a** (red). Conditions: 0.3 mM (acetone), 0.1 M Bu_4NPF_6, scan rate 0.05 V s^{-1}, room temperature.

*Determination of the pK_a of the O−H in **1**−**3a(H)**.* As of yet, we have been unable to synthesize the conjugate acid complexes **1**−**3a(H)** (i.e., $[Ni^{II}(H_2CO_3)(L)]$, $[Ni^{II}(HOAc)(L)]$, $[Ni^{II}(HNO_3)(L)]$). Upon reaction between AcOH or HNO_3 (1 equiv, room temperature) and complex **4**, the

DOI: 10.1021/jacs.6b08406
J. Am. Chem. Soc. 2016, 138, 14362−14370

complex decomposed to yield *N,N′*-bis(2,6-dimethylphenyl)-2,6-pyridinedicarboxamide, as evidenced by ^{1}H NMR spectroscopy (Figures S29 and S30). Similarly, electronic absorption and ^{1}H NMR analyses of the reaction between **2a** and either $Et_2O{\cdot}HBF_4$ or AcOH showed protonation and decomposition of the complex (Figures S31−33). We were thus unable to experimentally determine the pK_a values of **1**−**3a(H)** and in turn cannot calculate the $BDFE_{O-H}$ for **1**−**3a(H)**.

Discussion on the Relative HAT Reactivities of 1−*3b toward Phenols.* In considering the reaction between **1**−**3b** and phenols, the following factors were considered:

(a) On the ancillary ligands of **1**−**3b** ($^-$OAc, $^-OCO_2H$, $^-ONO_2$), there are multiple O-atoms that can be the acceptor/binding site of the incoming H-atom during the reaction between **1**−**3b** and 2,6-DTBP. It is also possible that rather than the ancillary O-atom donor, it is the carboxamido- N- or O-atom that accepts the proton. Given the stark differences in reactivity of **3b** compared to **1**/**2b**, we surmise the H-atom to be delivered to the ancillary ligand. While our reactivity studies indicated a (concerted) HAT reaction, that does not necessarily mean the proton and electron are delivered to the same location (Scheme 3). Arguments can be made for at least two mechanistic postulates (thus HAT or separated concerted proton and electron transfer), where the incoming proton either arrives at the proximal or distal O-atoms of the metal bound $^-OCO_2H$, $^-$OAc, and $^-ONO_2$ ligands in **1**−**3b**.[25]

Scheme 3. Possible PCET Mechanisms for the Reaction of Ni^{III}-Oxygen Adducts (Ni^{III}-Acetate Here) with Alcohols (ROH)[a]

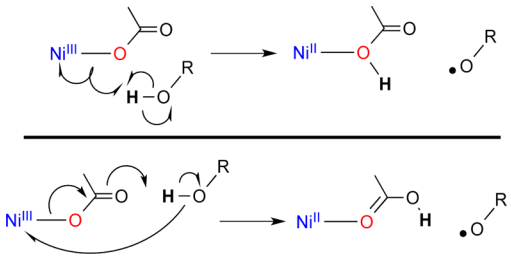

[a]Top: classical HAT mechanism. Bottom: separated concerted proton and electron transfer.

(b) According to cyclic voltammetry, **3a** displayed a higher $E^0_{Ni(II/III)}$ than **1**−**2a**, while XAS indicated that **3b** displayed the longest Ni−O bond length. These observations indicate that the $^-ONO_2$ ligand in **3b** is a relatively weak-field donor, and causes the Ni^{III}-oxygen adduct **3b** to be relatively more electrophilic.

(c) We were unable to determine the $BDFE_{O-H}$ in **1**−**3a(H)**, preventing an accurate comparison of the relative $BDFE_{O-H}$ to relative reactivity. Crictically, we cannot say with certainty that reaction of **1**−**3a** with H^+-donors would result in the same O-atom being protonated as reaction of **1**−**3b** with H-atom donors.

(d) HNO_3 is considerably more acidic than H_2CO_3 and AcOH. Based on this, we postulate that when comparing metal-bound HNO_3 to metal-bound H_2CO_3 and AcOH in **1**−**3a(H)**, that the pK_a of the HNO_3 in **3a(H)** will be lower than that for **1**−**2a(H)**.

(e) For free AcOH and HNO_3 the BDE_{O-H} are 112 and 101.7 kcal/mol, respectively.[26] To the best of our knowledge $BDE/BDFE_{O-H}$ of H_2CO_3 are yet to be predicted/determined. Based on the higher BDE_{O-H} value for AcOH, one would anticipate the acetoxyl radical to display higher rate constants for HAT than the nitro-oxyl radical. This contrasts with our observation that $^-ONO_2$-ligated **3b** displayed a higher k_2 than $^-$OAc-ligated **2b**, suggesting that the $BDFE_{O-H}$ in **3a(H)** is greater than that in **1a(H)** or **2a(H)**.

In summary, **3a** displayed a higher $E^0_{Ni(II/III)}$ than **1**−**2a**, and **3b** is postulated to be the most electrophilic oxidant, while **3a(H)** is postulated to contain a more acidic proton than **1**−**2a(H)**. **3b** displayed a higher k_2 for the oxidation of phenols, suggesting that the $BDFE_{O-H}$ in **3a(H)** is greater than that in **1**/**2a(H)**. Based on these observations, we surmise that in the reaction between **1**−**3b** and phenols, electron transfer has a greater contribution to HAT reaction rate than proton transfer. This is because the postulated relatively low pK_a value in **3a(H)** does not cause a relatively low reaction rate, whereas the relatively high $E^0_{Ni(II/III)}$ for **3a** appears to correlate with a higher oxidation rate for **3b**. We believe this is an interesting outcome, because it suggests the reactivity of high-valent oxidants may be tuned by simply tuning the electronic properties of the ancillary oxygen-atom donor ligand. Examples of either the effect of the redox potential[12e] or of basicity[27] prevailing have been observed in the literature, although the modifications in the complexes are not as simple as the substitution of a terminal oxygen-ligand.

Hydrocarbon Oxidation. At low temperatures (−40 °C), only 1-benzyl-1,4-dihydronicotinamide (BNAH, BDE = 68 kcal mol^{-1}) and 10-methyl-9,10-dihydroacridine (BDE = 74 kcal/mol),[28] were capable of bringing about the decay of **2b** and **3b** (i.e., were oxidized by **2b** and **3b**). At room temperature we explored the reactivity of **2b** toward hydrocarbon substrates with gradually increasing C−H bond strengths (BDE = 78−90 kcal/mol) including xanthene, 9,10-dihydroanthracene (DHA), fluorene, benzyl alcohol, ethylbenzene and toluene.[29] **2b** was found to react with all of the listed substrates at 25 °C, along time scales that allowed kinetic analysis of the reactions. We determined k_2 for the reaction of each of these substrates with **2b** using methods analogous to those described above for phenols (Table S4, Figures S35−S43).

A plot of the logarithms of the k_2 for the reaction of **2b** with each substrate against the substrate BDE_{C-H} showed a linear correlation (Figure 7).[30,31] This is what was expected for a HAT mechanism, in which BDEs determine the $\Delta H°$ of the reaction. Conversely, the correlations between k_2 and either pK_a

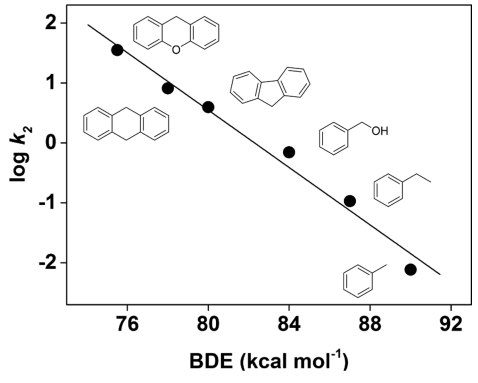

Figure 7. Plot of log(k_2), for the reactions of **2b** with hydrocarbon substrates, measured at 25 °C, against the BDE_{C-H} of the substrates. BDEs from ref 29. The reaction rate of DHA was corrected by a factor of 2 to account for the second HAT event from anthracenyl radical.

DOI: 10.1021/jacs.6b08406
J. Am. Chem. Soc. 2016, 138, 14362−14370

or reduction potentials $E^0_{Ni(II/III)}$ of the substrates are poor: the C−H bond of fluorene is more acidic than that of any of the other substrates, and xanthene is far more easily oxidized than the rest.[22] The observed linear relationship between reaction rate and BDE_{C-H} is thus a strong indication of a HAT rate-determining step. Deriving Gibbs energies of activation from the measured k_2 values, a $\Delta G^{\ddagger}/\Delta(BDE)$ slope of −0.31 can be determined (Figure S44). This value compares favorably with the $\Delta G^{\ddagger}/\Delta G°$ value of −0.5 predicted by Marcus theory,[12c,14] and experimental values in the range of −0.15−0.7 for other comparable complexes (Table 2).

Analysis of the post-reaction mixtures was conducted by GC-MS, and the identified oxidized products were consistent with HAT-initiated oxidation. Oxygenated products were formed from all substrates (xanthone from xanthene, anthraquinone from DHA, fluorenone from fluorene, benzoic acid from benzyl alcohol and toluene and acetophenone from ethylbenzene, Scheme S2). However, from the reaction of DHA with **2b**, the main product was the aromatized anthracene, with only traces on anthraquinone being formed. In no case did we find products incorporating chlorine or acetate moieties, demonstrating that the NaOCl/AcOH oxidant is not responsible for the substrate oxidation.[32,33]

To further investigate the mechanism of the reaction between **2b** and hydrocarbon substrates, we employed the deuterated substrates [D_2]xanthene and [D_4]DHA. The reactions with the deuterated substrates proceeded more slowly than with the corresponding protic substrates, giving kinetic isotope effect (KIE) values of 3.3 and 3.0 respectively (Figure S36). These values closely match the KIE value determined for the reaction between **1b** and 2,6-DTBP (2.1).[7] The presence of a primary kinetic isotope effect lends further evidence that C−H bond breaking occurs in the rate-determining step. The relatively small size of the effect could be explained by the high temperature of the experiment. Should the difference in activation energies be exactly equal to the difference between the zero-point energies of C−H and C−D stretching vibrations, a KIE of 6.9 would be predicted at 25 °C.[34] Lower values, as in the case of **1b** and **2b,** can arise from a not fully linear O···H···C reaction axis, or from a significant vibration involving the hydrogen atom in the transition state.[34a]

DHA is a commonly employed substrate in HAT studies, allowing us to compare the reactivity properties of **2b** to those of previously reported high-valent metal−oxygen adducts. We have tabulated the determined k_2 values for the reaction between DHA and selected complexes of Mn, Fe, Ru, and Cu at 25 °C (Table 2). The k_2 for **2b** was about half of that of $[Fe^{IV}(O)(N_4Py)]^{2+}$, and only 1 order of magnitude smaller than $[Ru^{IV}(O)(bpy)_2(py)]^{2+}$ and $[Cu^{III}(OH)(pyN_2^{iPr2})]$, which rank among the most reactive oxidants reported to date. Permanganate (MnO_4^-), as well as the Mn^{IV}-dioxo $[Mn^{IV}(Me_2EBC)(O)_2]$, are considerably slower. It should be noted that **2b** is not an oxo complex. By comparison, an Fe^{III}-alkoxide complex ($[Fe^{III}(OCH_3)(PY5)]^{2+}$) is a much weaker oxidant compared to Fe^{IV}═O. The high reaction rate of **2b**, as well as that of Tolman's Cu^{III}−OH complex, lend weight to the postulated high oxidizing power of complexes based on the late-transition metals.

CONCLUSIONS

We have synthesized and fully characterized two new $[Ni^{III}(OX)(L)]$ compounds, **2b** and **3b**, demonstrating the high-yield preparation of pure Ni^{III}-oxidants. Comparison of their oxidative reactivity towards 2,6-di-*tert*-butylphenol, showed the $^-ONO_2$ complex **3b** reacted 15 times faster than its ^-OAc and $^-OCO_2H$ congeners, indicating that the electron-deficiency of the complex is the prevalent factor in determining oxidizing potency. For **2b**, a linear Polanyi relationship between k_2 and substrate BDE_{C-H} provides strong evidence for the postulated HAT mechanism of C−H bond activation. **2b** was capable of reacting with relatively hard-to-oxidize substrates and has a high reaction rate toward DHA, of the same order of magnitude as Fe^{IV}═O complexes, in spite of the stabilization afforded by substitution at the O atom (thus carboxylato- versus oxo- complexes). This report demonstrates the effectiveness of late-transition metal oxidants in the activation of strong C−H bonds, and the ease at which the reactivity of high-valent metal−oxygen adducts can be tuned by simple manipulation of anionic constituents.

Table 2. Kinetic Parameters for the HAT Reactions of Selected High Valent Metal−Oxo and Other Metal−Oxygen Complexes with DHA[a]

	k_2[b] (M^{-1} s^{-1})	KIE[c]	$-\Delta G^{\ddagger}/\Delta(BDE)$[d]
2b	8.11	3.0	0.31
$[Mn^{VII}O_4]^-$[35]	0.12		0.69
$[Mn^{IV}(Me_2EBC)(O)_2]$[36]	∼0.03	3.78[e]	0.21
$[Fe^{IV}(O)(N_4Py)]^{2+}$[37]	18	20[f]	0.15
$[Fe^{III}(OCH_3)(PY5)]^{2+}$[38]	0.0049	5.5	0.17
$[Ru^{IV}(O)(bpy)_2(py)]^{2+}$[29a]	125	50−100	0.47
$[Cu^{III}(OH)(pyN_2^{iPr2})]^{5}$[5,12e]	∼190	24[g]	0.37

[a]Me_2EBC = 4,11-dimethyl-1,4,8,11-tetraazabicyclo[6.6.2]hexadecane, N_4Py = *N*,*N*-bis(2-pyridylmethyl)-bis(2-pyridyl)methylamine, PY5 = 2,6-bis(bis(2-pyridyl)methoxymethane)pyridine, bpy =2,2′-bipyridine, py = pyridine, pyN_2^{iPr2} = *N*,*N*′-bis(2,6-diisopropylphenyl)pyridine-2,6-dicarboxamidate. [b]For the reaction with DHA at 25 °C. For $[Mn^{IV}(Me_2EBC)(O)_2]$ and $[Cu^{III}(OH)(pyN_2^{iPr2})]$, data at 25 °C was not available; values were derived from the experimentally determined activation parameters via the Eyring equation. [c]Kinetic isotope effect for the oxidation of DHA, measured at 25 °C unless otherwise noted. [d]Empirically determined slope of the activation free energy vs substrate BDE regression line, for a series of hydrocarbon substrates. [e]Measured at 288 K. [f]Measured at 313 K. [g]measured at 248 K.

ASSOCIATED CONTENT

Supporting Information

The Supporting Information is available free of charge on the ACS Publications website at DOI: 10.1021/jacs.6b08406.

Experimental materials and procedures; electronic absorption, NMR, FTIR, MS, and EPR spectra; kinetic data; XAS methods and data analysis; DFT methods and calculated structures (PDF)
Crystal data for **2a** (CIF)
Crystal data for **3a** (CIF)
Crystal data for **4** (CIF)

AUTHOR INFORMATION

Corresponding Author

*aidan.mcdonald@tcd.ie

Notes

The authors declare no competing financial interest.

DOI: 10.1021/jacs.6b08406
J. Am. Chem. Soc. 2016, 138, 14362−14370

■ ACKNOWLEDGMENTS

This publication has emanated from research supported by the European Union (FP7-333948, ERC-2015-STG-678202). Research in the McDonald lab is supported in part by a research grant from Science Foundation Ireland (SFI/12/RC/2278), and in the Swart lab by the Ministerio de Economia y Competitividad (MINECO, Projects CTQ2014-59212-P and CTQ2015-70851-ERC), the DIUE of the Generalitat de Catalunya (Project 2014SGR1202), and the European Fund for Regional Development (FEDER, UNGI10-4E-801). XAS experiments were conducted at SSRL beamline 2-2 (SLAC National Accelerator Laboratory), with support from the DOE Office of Science (DE-AC02-76SF00515 and DE-SC0012704) and NIH (P30-EB-009998). We are grateful to: COST Action CM1305 (ECOSTBio) for networking support; Dr. Brendan Twamley for performing X-ray crystallography measurements; Dr. Anthony Fitzpatrick and Dr. Grace Morgan for EPR technical support; Chiara Cecchini for exploratory studies; Dr. Apparao Draksharapu and Prof. Wesley Browne for identifying NaOCl/AcOH as a useful oxidant.

■ REFERENCES

(1) Bordeaux, M.; Galarneau, A.; Drone, J. *Angew. Chem., Int. Ed.* **2012**, *51*, 10712−10723.
(2) Doble, M. V.; Ward, A. C. C.; Deuss, P. J.; Jarvis, A. G.; Kamer, P. C. J. *Bioorg. Med. Chem.* **2014**, *22*, 5657−5677.
(3) Huynh, M. H. V.; Meyer, T. J. *Chem. Rev.* **2007**, *107*, 5004−5064.
(4) (a) Yin, G. *Coord. Chem. Rev.* **2010**, *254*, 1826−1842. (b) Song, W. J.; Seo, M. S.; George, S. D.; Ohta, T.; Song, R.; Kang, M.-J.; Tosha, T.; Kitagawa, T.; Solomon, E. I.; Nam, W. *J. Am. Chem. Soc.* **2007**, *129*, 1268−1277. (c) Krebs, C.; Galonić Fujimori, D.; Walsh, C. T.; Bollinger, J. M. *Acc. Chem. Res.* **2007**, *40*, 484−492. (d) McDonald, A. R.; Que, L. *Coord. Chem. Rev.* **2013**, *257*, 414−428.
(5) Donoghue, P. J.; Tehranchi, J.; Cramer, C. J.; Sarangi, R.; Solomon, E. I.; Tolman, W. B. *J. Am. Chem. Soc.* **2011**, *133*, 17602−17605.
(6) (a) Huang, D.; Holm, R. H. *J. Am. Chem. Soc.* **2010**, *132*, 4693−4701. (b) Huang, D.; Makhlynets, O. V.; Tan, L. L.; Lee, S. C.; Rybak-Akimova, E. V.; Holm, R. H. *Proc. Natl. Acad. Sci. U. S. A.* **2011**, *108*, 1222−1227. (c) Huang, D.; Makhlynets, O. V.; Tan, L. L.; Lee, S. C.; Rybak-Akimova, E. V.; Holm, R. H. *Inorg. Chem.* **2011**, *50*, 10070−10081.
(7) Pirovano, P.; Farquhar, E. R.; Swart, M.; Fitzpatrick, A. J.; Morgan, G. G.; McDonald, A. R. *Chem. - Eur. J.* **2015**, *21*, 3785−3790.
(8) (a) Hikichi, S.; Yoshizawa, M.; Sasakura, Y.; Akita, M.; Moro-oka, Y. *J. Am. Chem. Soc.* **1998**, *120*, 10567−10568. (b) Itoh, S.; Bandoh, H.; Nagatomo, S.; Kitagawa, T.; Fukuzumi, S. *J. Am. Chem. Soc.* **1999**, *121*, 8945−8946. (c) Shiren, K.; Ogo, S.; Fujinami, S.; Hayashi, H.; Suzuki, M.; Uehara, A.; Watanabe, Y.; Moro-oka, Y. *J. Am. Chem. Soc.* **2000**, *122*, 254−262. (d) Itoh, S.; Bandoh, H.; Nakagawa, M.; Nagatomo, S.; Kitagawa, T.; Karlin, K. D.; Fukuzumi, S. *J. Am. Chem. Soc.* **2001**, *123*, 11168−11178. (e) Hikichi, S.; Yoshizawa, M.; Sasakura, Y.; Komatsuzaki, H.; Moro-oka, Y.; Akita, M. *Chem. - Eur. J.* **2001**, *7*, 5011−5028. (f) Schenker, R.; Mandimutsira, B. S.; Riordan, C. G.; Brunold, T. C. *J. Am. Chem. Soc.* **2002**, *124*, 13842−13855.
(9) Pfaff, F. F.; Heims, F.; Kundu, S.; Mebs, S.; Ray, K. *Chem. Commun.* **2012**, *48*, 3730−3732.
(10) Corona, T.; Pfaff, F. F.; Acuña-Parés, F.; Draksharapu, A.; Whiteoak, C. J.; Martin-Diaconescu, V.; Lloret-Fillol, J.; Browne, W. R.; Ray, K.; Company, A. *Chem. - Eur. J.* **2015**, *21*, 15029−15038.
(11) (a) Chmielewski, P. J.; Latos-Grażyński, L. *Inorg. Chem.* **1997**, *36*, 840−845. (b) Chiou, T.-W.; Liaw, W.-F. *Inorg. Chem.* **2008**, *47*, 7908−7913. (c) Zhou, W.; Schultz, J. W.; Rath, N. P.; Mirica, L. M. *J. Am. Chem. Soc.* **2015**, *137*, 7604−7607.
(12) (a) Gunay, A.; Theopold, K. H. *Chem. Rev.* **2010**, *110*, 1060−81. (b) Costas, M.; Mehn, M. P.; Jensen, M. P.; Que, L. *Chem. Rev.* **2004**, *104*, 939−986. (c) Mayer, J. M. *Acc. Chem. Res.* **2011**, *44*, 36−46. (d) Yiu, D. T. Y.; Lee, M. F. W.; Lam, W. W. Y.; Lau, T.-C. *Inorg. Chem.* **2003**, *42*, 1225−1232. (e) Dhar, D.; Yee, G. M.; Spaeth, A. D.; Boyce, D. W.; Zhang, H.; Dereli, B.; Cramer, C. J.; Tolman, W. B. *J. Am. Chem. Soc.* **2016**, *138*, 356−368.
(13) (a) Bell, R. P. *Proc. R. Soc. London, Ser. A* **1936**, *154*, 414−429. (b) Evans, M. G.; Polanyi, M. *Trans. Faraday Soc.* **1938**, *34*, 11−24.
(14) (a) Roth, J. P.; Yoder, J. C.; Won, T.-J.; Mayer, J. M. *Science* **2001**, *294*, 2524−2526. (b) Mayer, J. M. *J. Phys. Chem. Lett.* **2011**, *2*, 1481−1489.
(15) (a) Shiota, Y.; Yoshizawa, K. *J. Am. Chem. Soc.* **2000**, *122*, 12317−12326. (b) Winkler, J. R.; Gray, H. B. *Struct. Bonding (Berlin, Ger.)* **2011**, *142*, 17−28.
(16) (a) Kawamoto, T.; Prakash, O.; Ostrander, R.; Rheingold, A. L.; Borovik, A. *Inorg. Chem.* **1995**, *34*, 4294−4295. (b) Kawamoto, T.; Hammes, B. S.; Haggerty, B.; Yap, G. P.; Rheingold, A. L.; Borovik, A. *J. Am. Chem. Soc.* **1996**, *118*, 285−286. (c) Patra, A. K.; Mukherjee, R. *Inorg. Chem.* **1999**, *38*, 1388−1393. (d) Wasilke, J.; Wu, G.; Bu, X.; Kehr, G.; Erker, G. *Organometallics* **2005**, *24*, 4289−4297.
(17) (a) Haines, R. I.; McAuley, A. *Coord. Chem. Rev.* **1981**, *39*, 77−119. (b) Collins, T. J.; Nichols, T. R.; Uffelman, E. S. *J. Am. Chem. Soc.* **1991**, *113*, 4708−4709. (c) Jacobs, S. A.; Margerum, D. W. *Inorg. Chem.* **1984**, *23*, 1195−1201. (d) Stuart, J. N.; Goerges, A. L.; Zaleski, J. M. *Inorg. Chem.* **2000**, *39*, 5976−5984.
(18) (a) Lovecchio, F. V.; Gore, E. S.; Busch, D. H. *J. Am. Chem. Soc.* **1974**, *96*, 3109−3118. (b) Kruger, H. J.; Peng, G.; Holm, R. H. *Inorg. Chem.* **1991**, *30*, 734−742. (c) Alonso, P. J.; Falvello, L. R.; Forniés, J.; Martín, A.; Menjón, B.; Rodríguez, G. *Chem. Commun.* **1997**, *2*, 503−504. (d) Ottenwaelder, X.; Ruiz-García, R.; Blondin, G.; Carasco, R.; Cano, J.; Lexa, D.; Journaux, Y.; Aukauloo, A. *Chem. Commun.* **2004**, 504−505.
(19) (a) Colpas, G. J.; Maroney, M. J.; Bagyinka, C.; Kumar, M.; Willis, W. S.; Suib, S. L.; Mascharak, P. K.; Baidya, N. *Inorg. Chem.* **1991**, *30*, 920−928. (b) Kundu, S.; Pfaff, F. F.; Miceli, E.; Zaharieva, I.; Herwig, C.; Yao, S.; Farquhar, E. R.; Kuhlmann, U.; Bill, E.; Hildebrandt, P.; Dau, H.; Driess, M.; Limberg, C.; Ray, K. *Angew. Chem., Int. Ed.* **2013**, *52*, 5622−5626. (c) Cho, J.; Kang, H. Y.; Liu, L. V.; Sarangi, R.; Solomon, E. I.; Nam, W. *Chem. Sci.* **2013**, *4*, 1502−1508.
(20) (a) Davidson, G.; Choudhury, S. B.; Gu, Z.; Bose, K.; Roseboom, W.; Albracht, S. P. J.; Maroney, M. J. *Biochemistry* **2000**, *39*, 7468−7479. (b) Haumann, M.; Porthun, A.; Buhrke, T.; Liebisch, P.; Meyer-Klaucke, W.; Friedrich, B.; Dau, H. *Biochemistry* **2003**, *42*, 11004−11015.
(21) Cho, J.; Sarangi, R.; Annaraj, J.; Kim, S. Y.; Kubo, M.; Ogura, T.; Solomon, E. I.; Nam, W. *Nat. Chem.* **2009**, *1*, 568−572.
(22) Mayer, J. M. *Annu. Rev. Phys. Chem.* **2004**, *55*, 363−390.
(23) (a) Dasgupta, P. K.; Nara, O. *Anal. Chem.* **1990**, *62*, 1117−1122. (b) Pines, D.; Ditkovich, J.; Mukra, T.; Miller, Y.; Kiefer, P. M.; Daschakraborty, S.; Hynes, J. T.; Pines, E. *J. Phys. Chem. B* **2016**, *120*, 2440−2451.
(24) Ranney, A. P.; Ziemann, P. J. *J. Phys. Chem. A* **2016**, *120*, 2561−2568.
(25) (a) Manner, V. W.; Dipasquale, A. G.; Mayer, J. M. *J. Am. Chem. Soc.* **2008**, *130*, 7210−7211. (b) Warren, J. J.; Tronic, T. A.; Mayer, J. M. *Chem. Rev.* **2010**, *110*, 6961−7001.
(26) Blanksby, S. J.; Ellison, G. B. *Acc. Chem. Res.* **2003**, *36*, 255−263.
(27) Baglia, R. A.; Prokop-Prigge, K. A.; Neu, H. M.; Siegler, M. A.; Goldberg, D. P. *J. Am. Chem. Soc.* **2015**, *137*, 10874−10877.
(28) Matsuo, T.; Mayer, J. M. *Inorg. Chem.* **2005**, *44*, 2150−2158.
(29) (a) Bryant, J. R.; Mayer, J. M. *J. Am. Chem. Soc.* **2003**, *125*, 10351−10361. (b) Brandi, P.; Galli, C.; Gentili, P. *J. Org. Chem.* **2005**, *70*, 9521−9528.
(30) Bediako, D. K.; Surendranath, Y.; Nocera, D. G. *J. Am. Chem. Soc.* **2013**, *135*, 3662−3674.
(31) While the thermodynamic relationships are strictly meant to hold for free energies, it is often necessary to substitute BDEs for BDFEs, due to the limited availability of BDFE data in the literature.

DOI: 10.1021/jacs.6b08406
J. Am. Chem. Soc. 2016, 138, 14362−14370

(32) Draksharapu, A.; Angelone, D.; Quesne, M. G.; Padamati, S. K.; Gómez, L.; Hage, R.; Costas, M.; Browne, W. R.; de Visser, S. P. *Angew. Chem., Int. Ed.* **2015**, *54*, 4357−4361.
(33) The absence of acetate-containing products makes a rebound recombination mechanism unlikely, i.e., one in which HAT is followed by reaction of the resulting carbon-based radical with a ligand in the metal coordination sphere. More likely, water or dioxygen in the solution is the source of the oxygen groups in the oxygenated products. When the oxidation of xanthene was performed in the presence of 30 μL of $H_2{}^{18}O$, both [^{16}O]xanthone and [^{18}O]xanthone were identified in approximately 1:1 ratio by ESI-MS.
(34) (a) Westheimer, F. H. *Chem. Rev.* **1961**, *61*, 265−273. (b) Kwart, H. *Acc. Chem. Res.* **1982**, *15*, 401−408.
(35) (a) Mandal, D.; Ramanan, R.; Usharani, D.; Janardanan, D.; Wang, B.; Shaik, S. *J. Am. Chem. Soc.* **2015**, *137*, 722−733. (b) Mandal, D.; Shaik, S. *J. Am. Chem. Soc.* **2016**, *138*, 2094−2097.
(36) Yin, G.; Danby, A. M.; Kitko, D.; Carter, J. D.; Scheper, W. M.; Busch, D. H. *J. Am. Chem. Soc.* **2008**, *130*, 16245−16253.
(37) (a) Klinker, E. J.; Shaik, S.; Hirao, H.; Que, L. *Angew. Chem., Int. Ed.* **2009**, *48*, 1291−1295. (b) Wang, D.; Zhang, M.; Bühlmann, P.; Que, L. *J. Am. Chem. Soc.* **2010**, *132*, 7638−7644.
(38) Goldsmith, C. R.; Jonas, R. T.; Stack, T. D. P. *J. Am. Chem. Soc.* **2002**, *124*, 83−96.

DOI: 10.1021/jacs.6b08406
J. Am. Chem. Soc. 2016, 138, 14362−14370